Chemical Engineering Journal 162 (2010) 1067–1074

Contents lists available at ScienceDirect

Chemical Engineering Journal

journal homepage: www.elsevier.com/locate/cej

The influence of reactivation by hydration of spent SO_2 sorbents on their impact fragmentation in fluidized bed combustors

Fabio Montagnaro[a,*], Piero Salatino[b,c], Luciano Santoro[a], Fabrizio Scala[b]

[a] Dipartimento di Chimica, Università degli Studi di Napoli Federico II, Complesso Universitario di Monte Sant'Angelo, 80126 Napoli, Italy
[b] Istituto di Ricerche sulla Combustione, Consiglio Nazionale delle Ricerche, Piazzale Vincenzo Tecchio 80, 80125 Napoli, Italy
[c] Dipartimento di Ingegneria Chimica, Università degli Studi di Napoli Federico II, Piazzale Vincenzo Tecchio 80, 80125 Napoli, Italy

ARTICLE INFO

Article history:
Received 23 March 2010
Received in revised form 26 June 2010
Accepted 28 June 2010

Keywords:
Fluidized bed combustion
Desulphurization
Reactivation
Fragmentation
Attrition

ABSTRACT

The relationship between calcination/sulphation and attrition/fragmentation of calcium-based SO_2 sorbents in fluidized bed (FB) combustors has long been recognized, but only recently did attrition by impact receive due consideration. There is limited available information in the literature on the propensity of exhausted calcium-based sorbents to undergo high-velocity impact fragmentation after they have been reactivated by steam or water hydration. The present study addresses the relationship between hydration-induced reactivation of spent Ca-based sorbents and attrition by impact loading. The sorbent used in this work (a high-calcium Italian limestone) was pre-processed (sulphation at 850 °C in a lab-scale FB, water hydration for 3 h at 25 °C in a thermostatic bath, steam hydration for 3 h at 250 °C in a tubular reactor, dehydration at 850 °C in the FB) and subjected to impact tests in a purposely designed impact test rig, operated with particle impact velocities ranging from 4 to 45 m s^{-1}. The particle size distribution of the debris was worked out to define a fragmentation index and a probability density function of the size of generated fragments. The effect of hydration/reactivation of spent sorbent on propensity to undergo impact fragmentation was assessed, and results are discussed in the light of a mechanistic framework. It was observed that the prevailing particle breakage pattern was splitting/chipping for water-reactivated samples, disintegration for steam-reactivated samples. Characterization of sorbent microstructure by porosimetry and microscopic investigation on the reactivated samples highlighted a clear relationship between the extent of fragmentation and the cumulative specific volume of mesopores.

1. Overview

Removal of sulphur oxides from flue gases issuing from atmospheric fluidized bed (FB) combustors by absorption on calcium-based sorbents has been extensively investigated [1]. Particle sulphation most typically conforms to a core–shell sulphation pattern: a sharp reaction front establishes in the sorbent particles between the porous unreacted CaO core and a compact reacted $CaSO_4$ outer shell [2–6]. Extensive sulphation of the core is prevented by the onset of strong diffusional resistances to SO_2 migration across the shell. The degree of calcium conversion seldom exceeds 30–40%, so that over-stoichiometric sorbent feeding is required, resulting in increased production of solid waste. Reactivation of spent sorbents in order to enhance their desulphurization ability may be accomplished by either water or steam hydration [7–16]. The recovery of the SO_2 sorption ability is mainly due to the formation of $Ca(OH)_2$ upon hydration of unreacted CaO in the core of spent particles. The larger $Ca(OH)_2$ molar volume compared with that of CaO determines the swelling of the core and the consequent fissuring of the hard $CaSO_4$ shell, resulting into improved accessibility of SO_2 towards the unconverted core when the reactivated material is reinjected into the FB reactor. A second possible mechanism leading to the enhancement of the sulphur capture ability of the reactivated sorbent has been recently reported, and consists of sulphur redistribution throughout the particle cross-section promoted by hydration [9,11,13].

The influence of the progress of chemical reactions (calcination and sulphation) on attrition/fragmentation of calcium-based SO_2 sorbents in FB combustors has been extensively characterized [17–23]. These reactions bring about significant modifications of the mechanical properties of sorbent particles. In particular, the progress of sulphation significantly hinders the attrition rate, due to the formation of a tougher $CaSO_4$ outer shell. The extensive literature on attrition of granular solids in FB [24] suggests that in-bed attrition can be related to either surface wear or impact damage. Most of the published investigations on sorbent attrition during *in situ* SO_2 capture in FB refer to moderate bubbling test conditions, which emphasize the contribution due to surface wear. Only

* Corresponding author. Tel.: +39 081 674029; fax: +39 081 674090.
E-mail address: fabio.montagnaro@unina.it (F. Montagnaro).

1385-8947/$ – see front matter © 2010 Elsevier B.V. All rights reserved.
doi:10.1016/j.cej.2010.06.042

recently did attrition by impact damage in FB receive consideration [25–27]. Impact damage is related to high-velocity collisions between fluidized particles and targets, which can be either bed material or reactor walls/internals. High-velocity impact conditions are experienced by the particles in the grid (jetting) region of FB combustors. The exit region of the riser and the cyclone are other potential locations of impact damage of sorbent particles. Impact fragmentation may result into generation of coarse/non-elutriable and fine/elutriable fragments, depending on the collision intensity and on the mechanical response of the impacting particle. Sorbent pre-processing, *e.g.* by calcination and sulphation, was shown to significantly affect the extent and pattern of fragmentation due to impact [26,27]. In particular, the fragmentation behaviour of sulphated limestone is affected by its composite core/shell nature: impact loading is mostly withstood by the outer sulphate layer at moderate impact velocities, resulting in limited fragmentation; at high impact velocity, fragmentation is extensive and involves also the porous unreacted core of the particle. Finally, the nature of the limestone (and, in particular, the pore size distribution developed after its calcination) is likely to strongly influence the fragmentation tendency of the particles, as reported in [27].

As regards the attrition propensity of hydrated-reactivated spent sorbents, previous investigations have only partly disclosed the effect of reactivation on attrition, as they were focused on moderate bubbling test conditions which promoted surface wear and fragmentation as the key attrition processes [9,11,13,15]. In these studies it was concluded that both water and steam reactivation affected to a moderate extent sorbent attrition by surface wear. No information was instead provided as regards the propensity of reactivated Ca-based sorbents to undergo high-velocity impact fragmentation. The present study is directed to partly fill this gap, as it addresses the extent to which reactivation of a spent sorbent affects impact fragmentation.

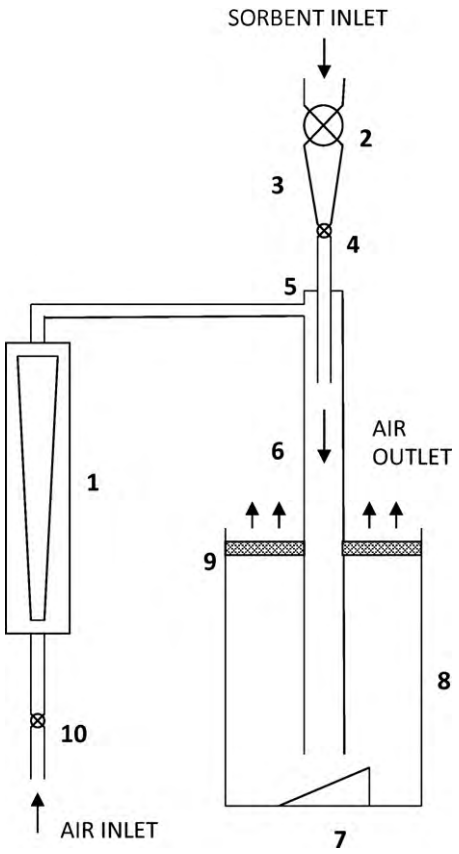

Fig. 1. Impact damage test apparatus (1 = gas flowmeter; 2 and 4 = lock hopper valves; 3 = hopper; 5 = feeding tube; 6 = eductor tube; 7 = target plate; 8 = collection chamber; 9 = cellulose filter; 10 = gas flow metering valve).

2. Experimental

2.1. Apparatuses

An electrically heated lab-scale stainless steel atmospheric bubbling FB reactor (40 mm ID and 1 m high) was used for sulphation and dehydration tests. The gas distributor was a perforated plate with 50 holes of 0.5 mm ID in a triangular pitch. On-line analysis of exhaust gases (SO_2, CO_2) was accomplished by NDIR gas analyzers. Further details on the experimental setup can be found elsewhere [11,19].

Steam hydration of spent sorbents was carried out in a stainless steel tubular reactor (Nabertherm B170, 27 mm ID), electrically heated for a length of 0.8 m. Water hydration was carried out by soaking spent sorbent in a thermostatic bath (Haake DC50).

Fragmentation by impact loading was characterized by means of a purposely designed experimental apparatus shown in Fig. 1. Sorbent particles are entrained in a gas stream and then impacted at controlled velocity against a target [20,25–31]. The test rig consists of a vertical stainless steel eductor tube (10 mm ID and 1 m high) equipped with a particle feeding device (a stainless steel hopper). The gas (air) enters the top section of the eductor tube and flows downward. The particle velocity at the impact is controlled by regulating the air flow in the eductor tube by means of a flowmeter. When the particles exit the eductor tube, they impact on a rigid target plate (made of stainless steel and inclined by 30°) placed in a glass collection chamber 50 mm below the bottom end of the tube. Air leaves the collection chamber from the top section after flowing through a porous cellulose filter where finer particulates are collected. The coarser impacted particles settle at the bottom, whence they are retrieved for further analysis.

2.2. Techniques

Characterization of sorbent particles was accomplished with the following methods:

(a) X-ray diffraction (XRD), by means of a Philips PW1710 diffractometer, with a diffraction angle ranging from 5° to 60° 2θ Cu Kα. XRD aimed at qualitative identification of the main crystalline phases in the samples.
(b) Mercury porosimetry, by means of a Carlo Erba P2000 porosimeter able to detect pore widths down to 4 nm. Porosimetric data were worked out to obtain the pore size distribution and, in particular, the cumulative pore volume of mesopores, defined as the pores having width up to 50 nm.
(c) Scanning electron microscopy (SEM), by means of a Philips XL30 microscope, aimed at qualitative inspection of particles morphology.

2.3. Procedures

The sorbent used in the experiments was a high-calcium Italian limestone (Massicci). Attrition under moderate bubbling test conditions of this limestone was characterized in Scala et al. [9,19]. Water and steam hydration of exhausted Massicci were characterized in Montagnaro et al. [11,13,15].

The experimental campaign was based on the characterization of samples of limestone pre-processed according to the steps outlined in Fig. 2 and described as follows.

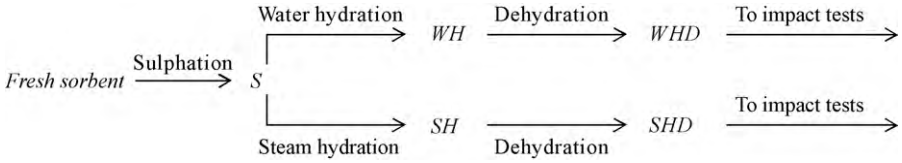

Fig. 2. Outline of the sample preparation protocol.

2.3.1. Sulphation (S)

Sulphation of limestone was carried out until exhaustion (batchwise at 850 °C) in the FB reactor. The bed material consisted of mixtures of limestone (20 g, 0.4–0.6 mm) and silica sand (150 g, 0.85–1 mm), fluidized at 0.75 m s^{-1} (the incipient fluidization velocity of the bed material is 0.3 m s^{-1} at 850 °C) with a gaseous stream containing SO_2 (1800 ppmv), O_2 (17.4%v) and N_2 (balance). Under these operating conditions, a sulphation time of 3 h was sufficient to make the sorbent particles fully exhausted. At the end of *S* tests, the exhausted sorbent was discharged from the bed and sieved out of the sand. The final degree of calcium conversion in *S* particles was 27.7%. Microscopic investigation of particle cross-sections demonstrated that the limestone was sulphated according to a prevailing core–shell pattern [11].

2.3.2. Water hydration-reactivation (WH)

S particles were reactivated by water hydration in the thermostatic bath, at 25 °C for a curing time of 3 h. To this end, batches of sulphated samples (10 g) blended with a large excess of distilled water (liquid/solid mass ratio = 25) were charged to sealed polyethylene bags and put in the thermostatic bath. At the end of the *WH* experiments, samples were retrieved from the apparatus, vacuum filtered and stored overnight at 110 °C in a desiccator.

2.3.3. Steam hydration-reactivation (SH)

S particles were reactivated by steam hydration in the tubular reactor, at 250 °C for 3 h. To this end, batches of sulphated samples (2 g) were charged in a ceramic holder and put into the reactor. Steam was continuously fed to the reactor at a flow rate of 0.144 m^3 h^{-1} (at 250 °C), a value largely over-stoichiometric when compared with the unconverted calcium present in the *S* sample. At the end of the *SH* experiments, samples were retrieved from the apparatus, vacuum filtered and stored overnight at 110 °C in a desiccator.

2.3.4. Dehydration on water hydrated (WHD) and steam hydrated (SHD) sorbent particles

When reactivated particles (either *WH* or *SH*) are reinjected in the hot FB, a very rapid loss of steam due to the decomposition of $Ca(OH)_2$ to CaO occurs, yielding the samples denoted as *WHD* and *SHD*, respectively. As the release of moisture and inherent water is usually very fast as compared to sulphation, it can be assumed that *WHD* and *SHD* samples are representative of the actual sorbent undergoing resulphation once reactivated sorbent is reinjected into the fluidized bed combustor. Accordingly, impact damage of *WHD* and *SHD* samples was characterized in the present study, rather than that of the less representative *WH* and *SH*. *WHD* and *SHD* samples were generated by dehydrating *WH* and *SH* samples at 850 °C for 10 min in the FB reactor. The bed was fluidized with air at 0.75 m s^{-1}.

2.3.5. Impact tests

Samples (1.5 g) of either *WHD* or *SHD* particles, sieved in the particle size range 0.4–0.6 mm, were fed to the impact test apparatus (Fig. 1) operated at ambient temperature. The particle impact velocity v was calculated as the sum of the gas velocity in the eductor tube and the particle terminal velocity. Simple calculations and experimental particle tracking (with the aid of a high-speed videocamera) indicated that particle acceleration to this velocity was complete well before impact. The tests were carried out for values of v ranging from 4 to 45 m s^{-1}. These velocities were selected so as to reproduce impact conditions that are likely to occur near the gas distributor of industrial-scale FB combustors. After the impact tests, *WHD* and *SHD* particles were retrieved from the collection chamber and weighed. The estimation of the material loss during the impact tests was carried out by mass balance. Loss of material was always within 3% of the initial sample weight. The collected samples were then characterized by granulometric analysis performed by mechanical sieving. To this end, a probability density function (PDF) of the sizes of particles collected after the impact was defined as:

$$PDF(d_i) = \frac{x(d_i)}{w(d_i)} \quad (1)$$

where x is the fractional mass of particles in a given size range (having d_i as mean diameter) and w is the width of that size range.

3. Results and discussion

Fig. 3a and b shows the XRD spectra for *WH* and *SH* particles, respectively: only $Ca(OH)_2$ (portlandite) as hydration product and $CaSO_4$ (anhydrite) as unconverted species were detected. The absence of lime indicates complete $CaO \Rightarrow Ca(OH)_2$ conversion, while the presence of anhydrite is consistent with the negligible rate of $CaSO_4$ hydration reactions under the operating conditions tested. XRD analysis for *WHD* and *SHD* particles are reported in Fig. 3c and d, respectively. The stronger signal is that related to the presence of lime deriving from $Ca(OH)_2$ decomposition, besides anhydrite and a minor signal for quartz related to sand impurities. The weak portlandite signals observable for *WHD* could be related to some CaO weathering effect after FB dehydration.

Figs. 4a and 5a report the cumulative particle size distributions of *WHD* and *SHD* samples, respectively, impacted at different velocities. In this work, all the collected particles (after impact) whose size falls below the lower limit of the feed size interval (0.4 mm) are classified as *fragments*. It is noted that the amount of fragments formed after one impact against the target increases with v, even if, for *WHD*, this tendency is less evident for $v < 24$ m s^{-1}.

Figs. 4b and 5b show the PDF of the fragment sizes for *WHD* and *SHD* samples, respectively, collected after impact tests. The particle breakage pattern can be directly linked to the PDF of the impacted samples [26]. With reference to the scheme of Fig. 6, it is recalled here that:

(a) *Particle chipping* is associated with the generation of a limited number of fragments of a size much smaller than that of the parent particle.
(b) *Particle splitting* is associated with the breakage of a particle into a relatively small number of fragments of a size comparable with that of the parent particle.
(c) *Particle disintegration* is associated with an extensive loss of particle connectivity, which results in the generation of a large number of small fragments, possibly reflecting the natural grain size [32] of the parent particle.

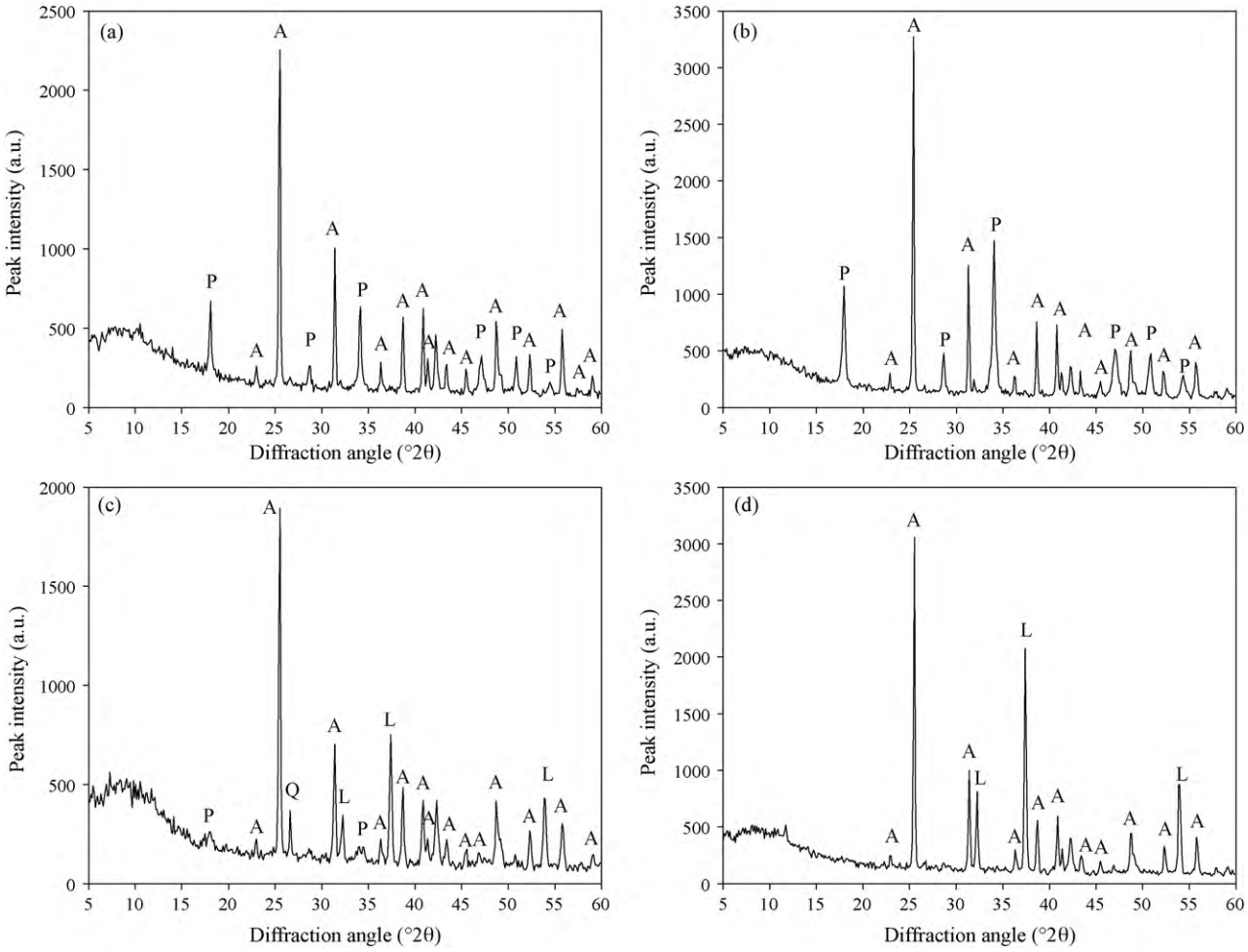

Fig. 3. XRD spectra of: (a) *WH*; (b) *SH*; (c) *WHD*; (d) *SHD* samples (A = anhydrite, $CaSO_4$; L = lime, CaO; P = portlandite, $Ca(OH)_2$; Q = quartz, SiO_2).

For brittle or semibrittle materials, impact generates cracks close to the contact point at the impact, which eventually propagate within the particle. If the energy associated with the impact is small (small v), crack propagation is confined within a region close to the particle surface, eventually bending toward the particle surface and resulting in chipping. For larger values of the impact energy, crack propagation extends across the whole particle, which eventually undergoes splitting [33]. For softer materials, particles breakage could more likely take place according to a disintegration pattern.

From inspection of Fig. 4b, it can be observed that the prevailing breakage pattern for *WHD* is particle splitting, possibly combined

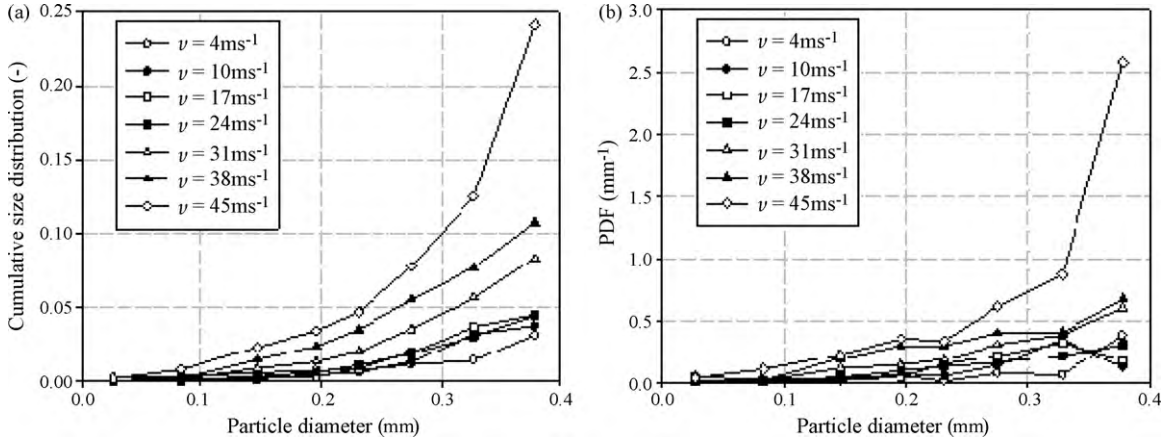

Fig. 4. Cumulative size distribution (a) and probability density function of particle size (b) of fragments collected after impact of *WHD* particles at different velocities (initial particle size range 0.4–0.6 mm).

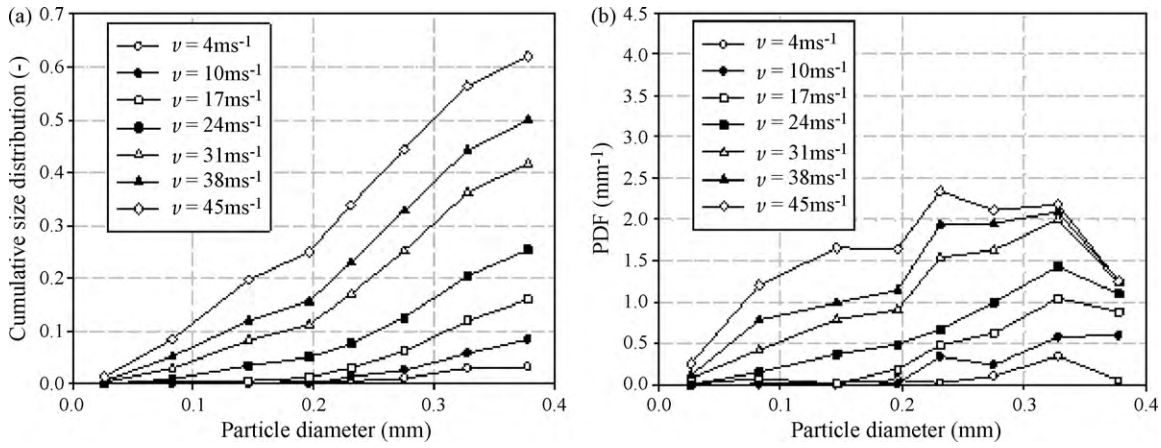

Fig. 5. Cumulative size distribution (a) and probability density function of particle size (b) of fragments collected after impact of *SHD* particles at different velocities (initial particle size range 0.4–0.6 mm).

with a certain degree of chipping. On the contrary, curves in Fig. 5b highlight a breakage pattern conforming to a disintegration mechanism for *SHD* samples (see Fig. 6).

To quantify the tendency of particles to undergo impact damage, it is useful to report the mass fractions of fragments f, defined as the total fraction of fragments cumulatively collected after impact:

$$f = \sum_{d_i=0}^{d_i=0.4\,\mathrm{mm}} x(d_i) \qquad (2)$$

as a function of v for *WHD* and *SHD* samples. These data are shown in the double-logarithmic plot of Fig. 7, chosen to better highlight the occurrence of power-law f versus v relationships ($f \propto v^k$), as frequently found by other authors [34,35].

For *WHD*, f increases from 3.1% ($v = 4\,\mathrm{m\,s^{-1}}$) to 24.1% ($v = 45\,\mathrm{m\,s^{-1}}$), displaying a transition at $v = 24\,\mathrm{m\,s^{-1}}$, marked by a pronounced change of the slope of the plot (*i.e.*, of the power-law index k). Most likely this corresponds to the point at which impact fragmentation by splitting becomes dominant.

It is interesting to compare the fragmentation pattern of *WHD* sample with that previously observed for the *S* sample [26]. Both are reported in Fig. 7. In the comparison, one should consider that *WHD* preserves the very same chemical structure ($CaSO_4$ concentrated in the outer shell, CaO in the inner core) of *S* particles, whereas the microstructural properties of *WHD* samples have been affected by the hydration-dehydration steps. At small values of v, the fractional mass of fragments f for *WHD* is larger than for *S*, consistently with the hypothesis that the hydration/dehydration treatment somewhat weakens the particle outer shell. At large impact velocities v the two curves are very close to each other, suggesting that the two samples display comparable mechanical resistance to the most energetic impacts. This might be explained in terms of the relative contribution to the mechanical resistance due to the outer shell versus the inner core of the particle. Under high-velocity impact conditions the whole particle withstands the mechanical stresses induced by impact, so that the apparent mechanical resistance of *WHD* and *S* samples is comparable, and the effect of microstructural differences confined in the outer layer vanishes.

When the extent of fragmentation of *SHD* samples is analyzed, it is found that increasing the impact velocity brings about a pronounced increase of f (from 3.2% at $v = 4\,\mathrm{m\,s^{-1}}$ to 62.1% at $v = 45\,\mathrm{m\,s^{-1}}$) associated with a remarkable change of attrition pattern

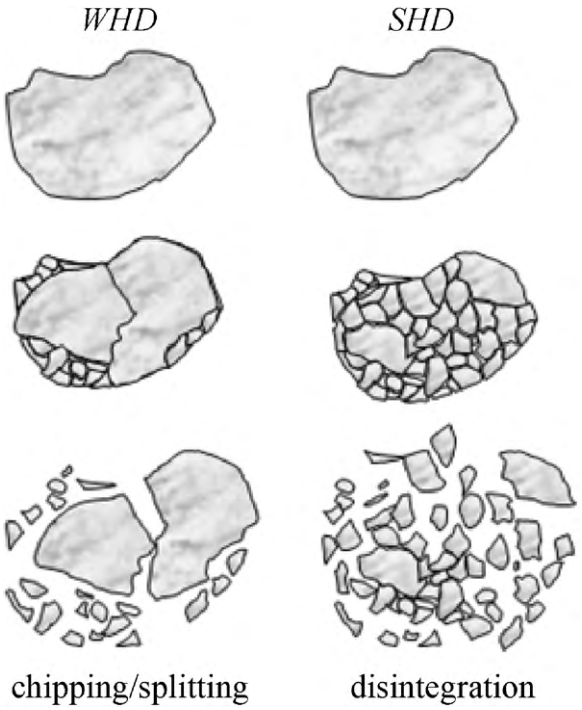

Fig. 6. Impact fragmentation patterns of *WHD* and *SHD* samples.

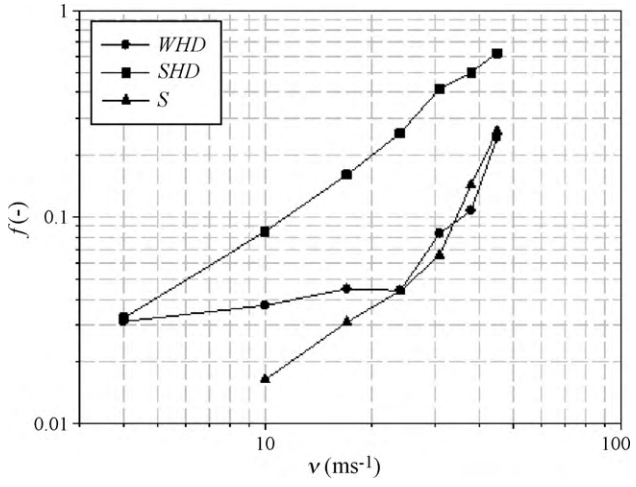

Fig. 7. Relationship between the fractional mass of fragments f and the impact velocity v for *WHD*, *SHD* and *S* particles.

Table 1
Cumulative specific mesopore volume for *WHD*, *SHD* and *S* samples.

Sample	Mesoporosity ($mm^3\ g^{-1}$)
WHD	31.0
SHD	195.0
S	32.5

(Fig. 7). In fact, large values of f obeying a power–law relationship over the entire range of impact velocities investigated are found, consistent with the disintegration failure pattern typical of soft materials. Comparison of f-values measured with *WHD* and *SHD* samples suggests that (except for the smallest v investigated) *SHD* samples are always more prone to undergo impact breakage than *WHD* samples. Moreover, even if the *SHD* chemical composition is not much different from those of *WHD* and *S* samples, its fragmentation pattern appears completely different from that of the other two samples. Interestingly, at very low impact velocity *WHD* and *SHD* samples give very similar impact fragmentation results, indicating that the sulphur-rich sorbent surface layer displays comparable mechanical resistance after the two different treatments. This result is consistent with the previous finding that the attrition rates by surface wear under moderate bubbling FB conditions of *WHD* and *SHD* samples are very close to each other [9,11,13,15].

One key to the attrition propensity of the different samples is represented by their microstructural properties, which have been analyzed by porosimetric characterization. Table 1 reports the values of mesoporosity of *S*, *WHD* and *SHD* samples. The cumulative mesopore volumes of *WHD* and *S* samples are fairly close to each other (about $30\ mm^3\ g^{-1}$), while *SHD* is much more porous

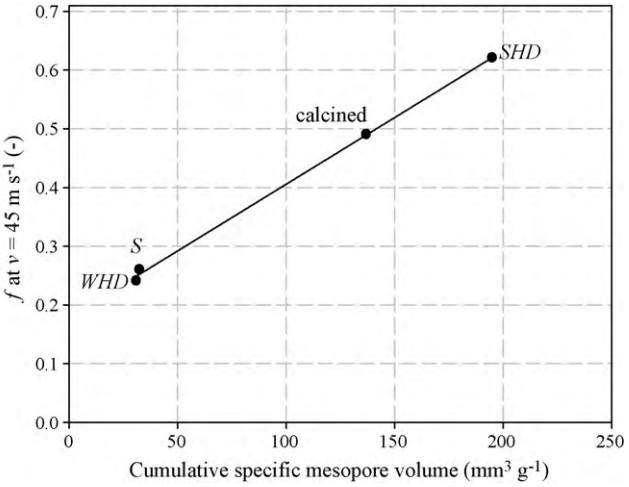

Fig. 8. Relationship between cumulative specific mesopore volume and fractional mass of fragments f at $v = 45\ m\ s^{-1}$ for different sorbent samples.

($195\ mm^3\ g^{-1}$). This could be related to low-temperature 'cramming' phenomena, induced by the water treatment and responsible for a reduced porosity of *WHD* particles [11]. A close correlation could be established between impact attrition at high v and mesopore volume of *S*, *WHD* and *SHD* samples, which extends also to the corresponding properties of the calcined limestone (investigated in Scala et al. [26]). This correlation is reported in Fig. 8. The fair correlation between the extent of attrition f and the cumula-

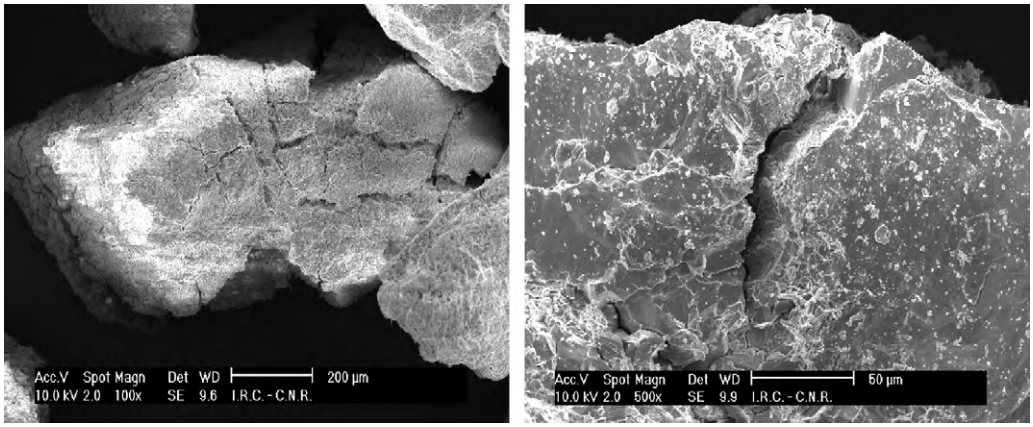

Fig. 9. SEM micrographs of *WHD* samples.

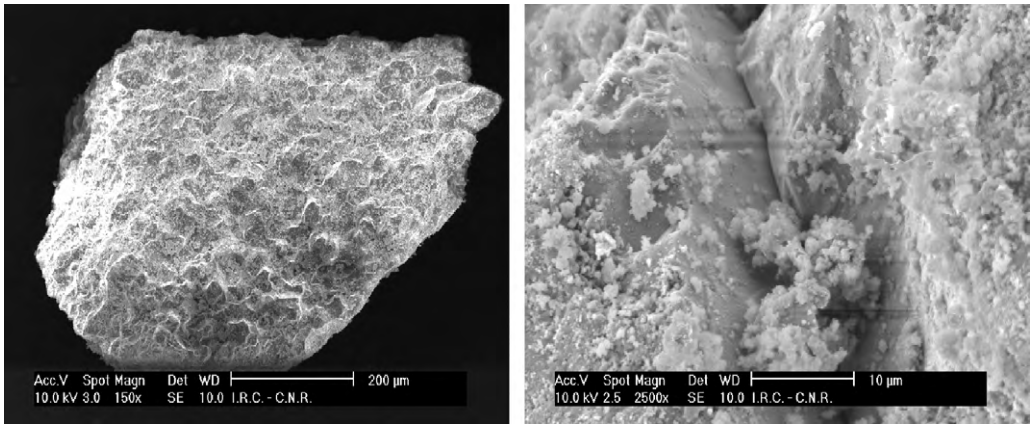

Fig. 10. SEM micrographs of *SHD* samples.

tive mesopore volume is consistent with the view that under the most energetic impact conditions the bulk properties of the sorbent particles, and in particular their mesoporosity, is one key to fragmentation by impact.

Microstructural characterization of *WHD* and *SHD* was complemented by SEM analysis. Micrographs of selected samples are reported in Figs. 9 and 10. *WHD* samples display a relatively compact structure, with only few superficial cracks. *SHD* samples have a different appearance, as they look more porous and corrugated. These features are consistent with the results of porosimetric analysis and with the fragmentation extent and pattern of the two types of samples.

Altogether, experimental results indicate that impact fragmentation of reactivated sorbent particles is extensive, especially at the highest impact velocities investigated. The consequences of fragmentation on exploitation of reactivated sorbent after reinjection in the fluidized bed are not trivial. On the one hand, particle breakage can lead to undesired loss of sorbent material by elutriation during resulphation. On the other hand, contacting the unreacted core of the particles with the reacting atmosphere can be enhanced by fragmentation, so that resulphation can take place more effectively. The competition between these conflicting effects in real FB combustors is affected by a combination of sorbent properties and operational parameters of the combustor which concur in determining the inventory and the particle size distribution of sorbent particles establishing at steady state in the bed, as reported in Montagnaro et al. [36]. Implementation of impact fragmentation data of reactivated sorbents collected in the present study into comprehensive population balance models of sorbent particles will be the subject of forthcoming research activities.

4. Conclusions

Reactivation of the desulphurization ability of spent calcium-based sorbents from fluidized bed combustors may be effectively accomplished by hydration with either water or steam. Hydration brings about modifications in the attrition propensity of the sorbent. The effect of reactivation on attrition by surface wear and on fragmentation under moderate bubbling fluidization conditions has been already documented in the literature. The fragmentation of a high-calcium sorbent reactivated by either water or steam hydration under high-velocity impact conditions has been characterized in the present study. The raw sorbent was pre-processed (sulphated, reactivated by either water or steam, dehydrated) and subjected to tests in a purposely designed apparatus in which sorbent particles could be impacted against a rigid target at velocities ranging from 4 to 45 m s^{-1}.

Results showed that the total fraction of fragments cumulatively collected after one impact with the target increases with the impact velocity, up to 24.1% and 62.1% (at impact velocity of 45 m s^{-1}) for water- and steam-reactivated samples, respectively. Different breakage patterns were observed depending on sorbent pre-processing. The prevailing fragmentation pattern was splitting/chipping (with a prevailing fractional mass of relatively coarse fragments) for water-reactivated samples. It was disintegration (with extensive generation of fine fragments) for steam-reactivated samples.

The extent and pattern of sorbent fragmentation was successfully correlated with the microstructural properties of the pre-processed samples, assessed via mercury porosimetry. In particular, the maximum extent of particle fragmentation was directly linked to the cumulative mesopore volume of either spent or reactivated samples. The correlation was further supported by microstructural characterization obtained by microscopic inspection of the different samples, which revealed a more porous and corrugated nature of steam-reactivated samples as compared with water-reactivated ones.

Acknowledgements

The authors are grateful to Mr. Sabato Russo, Ms. Grazia Accardo and Mr. Gennaro Somma for their support in the experimental campaign.

References

[1] E.J. Anthony, D.L. Granatstein, Sulfation phenomena in fluidized bed combustion systems, Prog. Energy Combust. Sci. 27 (2001) 215–236.
[2] K. Dam-Johansen, K. Østergaard, High-temperature reaction between sulphur dioxide and limestone. I. Comparison of limestones in two laboratory reactors and a pilot plant, Chem. Eng. Sci. 46 (1991) 827–837.
[3] K. Dam-Johansen, K. Østergaard, High-temperature reaction between sulphur dioxide and limestone. II. An improved experimental basis for a mathematical model, Chem. Eng. Sci. 46 (1991) 839–845.
[4] F. Montagnaro, P. Salatino, F. Scala, The influence of sorbent properties and reaction temperature on sorbent attrition, sulfur uptake, and particle sulfation pattern during fluidized-bed desulfurization, Combust. Sci. Technol. 174 (2002) 151–169.
[5] W. Duo, K. Laursen, J. Lim, J.R. Grace, Crystallization and fracture: product layer diffusion in sulfation of calcined limestone, Ind. Eng. Chem. Res. 43 (2004) 5653–5662.
[6] F. Montagnaro, P. Salatino, F. Scala, The influence of temperature on limestone sulfation and attrition under fluidized bed combustion conditions, Exp. Therm. Fluid Sci. 34 (2010) 352–358.
[7] M.F. Couturier, D.L. Marquis, F.R. Steward, Y. Volmerange, Reactivation of partially-sulphated limestone particles from a CFB combustor by hydration, Can. J. Chem. Eng. 72 (1994) 91–97.
[8] K. Laursen, W. Duo, J.R. Grace, J. Lim, Sulfation and reactivation characteristics of nine limestones, Fuel 79 (2000) 153–163.
[9] F. Scala, F. Montagnaro, P. Salatino, Enhancement of sulfur uptake by hydration of spent limestone for fluidized-bed combustion application, Ind. Eng. Chem. Res. 40 (2001) 2495–2501.
[10] K. Laursen, W. Duo, J.R. Grace, J. Lim, Cyclic steam reactivation of spent limestone, Ind. Eng. Chem. Res. 43 (2004) 5715–5720.
[11] F. Montagnaro, F. Scala, P. Salatino, Reactivation by water hydration of spent sorbent for fluidized-bed combustion application: influence of hydration time, Ind. Eng. Chem. Res. 43 (2004) 5692–5701.
[12] D. Góra, E.J. Anthony, E.M. Bulewicz, L. Jia, Steam reactivation of 16 bed and fly ashes from industrial-scale coal-fired fluidized bed combustors, Fuel 85 (2006) 94–106.
[13] F. Montagnaro, F. Pallonetto, P. Salatino, F. Scala, Steam reactivation of a spent sorbent for enhanced SO_2 capture in FBC, AIChE J. 52 (2006) 4090–4098.
[14] E.J. Anthony, E.M. Bulewicz, L. Jia, Reactivation of limestone sorbents in FBC for SO_2 capture, Prog. Energy Combust. Sci. 33 (2007) 171–210.
[15] F. Montagnaro, P. Salatino, F. Scala, R. Chirone, An assessment of water and steam reactivation of a fluidized bed spent sorbent for enhanced SO_2 capture, Powder Technol. 180 (2008) 129–134.
[16] F. Montagnaro, M. Nobili, A. Telesca, G.L. Valenti, E.J. Anthony, P. Salatino, Steam hydration-reactivation of FBC ashes for enhanced in situ desulphurization, Fuel 88 (2009) 1092–1098.
[17] R.R. Chandran, J.N. Duqum, Attrition characteristics relevant for fluidized bed combustion, in: J.R. Grace, L.W. Shemilt, M.A. Bergougnou (Eds.), Fluidization VI, Engineering Foundation, New York, 1989, pp. 571–580.
[18] M.F. Couturier, I. Karidio, F.R. Steward, Study on the rate of breakage of various Canadian limestones in a circulating transport reactor, in: A.A. Avidan (Ed.), Circulating Fluidized Bed Technology IV, American Institute of Chemical Engineers, New York, 1993, pp. 672–678.
[19] F. Scala, A. Cammarota, R. Chirone, P. Salatino, Comminution of limestone during batch fluidized-bed calcination and sulfation, AIChE J. 43 (1997) 363–373.
[20] F. Scala, P. Salatino, R. Boerefijn, M. Ghadiri, Attrition of sorbents during fluidized bed calcination and sulphation, Powder Technol. 107 (2000) 153–167.
[21] J.J. Saastamoinen, T. Shimizu, Attrition-enhanced sulfur capture by limestone particles in fluidized beds, Ind. Eng. Chem. Res. 46 (2007) 1079–1090.
[22] K. Redemann, E.U. Hartge, J. Werther, Ash management in circulating fluidized bed combustors, Fuel 87 (2008) 3669–3680.
[23] J. Saastamoinen, T. Pikkarainen, A. Tourunen, M. Räsänen, T. Jäntti, Model of fragmentation of limestone particles during thermal shock and calcination in fluidised beds, Powder Technol. 187 (2008) 244–251.
[24] J. Werther, J. Reppenhagen, Attrition, in: W.C. Yang (Ed.), Handbook of Fluidization and Fluid-Particle Systems, Dekker, New York, 2003, pp. 201–237.
[25] Z. Chen, J. Lim, J.R. Grace, Study of limestone particle impact attrition, Chem. Eng. Sci. 62 (2007) 867–877.
[26] F. Scala, F. Montagnaro, P. Salatino, Attrition of limestone by impact loading in fluidized beds, Energy Fuels 21 (2007) 2566–2572.
[27] F. Scala, F. Montagnaro, P. Salatino, Sulphation of limestones in a fluidized bed combustor: the relationship between particle attrition and microstructure, Can. J. Chem. Eng. 86 (2008) 347–355.

[28] K.R. Yuregir, M. Ghadiri, R. Clift, Observations on impact attrition of granular solids, Powder Technol. 49 (1986) 53–57.
[29] R.P. Davuluri, T.M. Knowlton, Development of a standardized attrition test procedure, in: L.S. Fan, T.M. Knowlton (Eds.), Fluidization IX, Engineering Foundation, New York, 1998, pp. 333–340.
[30] A.D. Salman, C.A. Biggs, J. Fua, I. Angyal, M. Szabó, M.J. Hounslow, An experimental investigation of particle fragmentation using single particle impact studies, Powder Technol. 128 (2002) 36–46.
[31] A. Samimi, R. Moreno, M. Ghadiri, Analysis of impact damage of agglomerates: effect of impact angle, Powder Technol. 143 (2004) 97–109.
[32] Y. Ray, T.S. Jiang, C.J. Wen, Particle attrition phenomena in a fluidized bed, Powder Technol. 49 (1987) 193–206.
[33] D.G. Papadopoulos, M. Ghadiri, Impact breakage of poly-methylmethacrylate (PMMA) extrudates. 1. Chipping mechanism, Adv. Powder Technol. 7 (1996) 183–197.
[34] M. Ghadiri, Z. Zhang, Impact attrition of particulate solids. Part 1: a theoretical model of chipping, Chem. Eng. Sci. 57 (2002) 3659–3669.
[35] Z. Zhang, M. Ghadiri, Impact attrition of particulate solids. Part 2: experimental work, Chem. Eng. Sci. 57 (2002) 3671–3686.
[36] F. Montagnaro, P. Salatino, F. Scala, M. Urciuolo, Sorbent inventory and particle size distribution in air-blown circulating fluidized bed combustors: the influence of particle attrition and fragmentation, in: G. Yue, H. Zhang, C. Zhao, Z. Luo (Eds.), Proceedings of the 20th International Conference on Fluidized Bed Combustion, Xi'an, China, 2009, pp. 966–971.